Fuel Processing Technology 226 (2022) 107093

Contents lists available at ScienceDirect

Fuel Processing Technology

journal homepage: www.elsevier.com/locate/fuproc

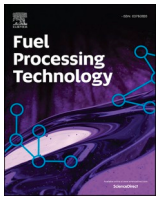

Research article

Combustion characteristics of aromatic-enriched oil droplets produced by pyrolyzing unrecyclable waste tire rubber

Yiliu Zhong [a], Jun Xu [b], Yuhan Pan [a], Zhitong Yin [a], Xinwen Wang [b], Yonggang Zhou [a], Qunxing Huang [a,*]

[a] State Key Laboratory of Clean Energy Utilization, Institute for Thermal Power Engineering, Zhejiang University, Hangzhou 310027, China
[b] Hangzhou Zhongce Rubber Cycle Technology Company Limited, Hangzhou 310000, Zhejiang, China

ARTICLE INFO

Keywords:
Waste tire pyrolysis
Condensed oil
Droplet combustion
Parameter calculation

ABSTRACT

The purpose of this work is to study the combustion characteristics of aromatic-enriched tire pyrolysis oil (TPO) produced from typical small vehicles and truck tires. Pyrolysis oils (NRTO: natural rubber tire oil and SRTO: synthetic rubber tire oil) from two raw radial tire materials were produced and condensed at 25 °C and 130 °C in a three-stage auger pyrolysis reactor under negative pressure. Combustion particularities were acquired using a single-droplet suspension combustion device and evaluated by five different indicators: kinetics, flame shape, burning rates, flame stand-off ratio (FSR) and mass transfer parameters. It was found that TPO was a potential fuel with higher calorific value (40–44 MJ/kg) and lower combustion apparent activation energy (10–40 MJ/mol) than that of bio-oil and solid fuels. Oil produced from synthetic rubber and condensed at 25 °C exhibited higher stable burning rate (1.93 ± 0.03 mm^2/s) than that of nature rubber pyrolysis oil. Comparing with traditional fuels, tire oil droplets displayed higher surface local heat transfer coefficient, but the mass transfer number (B ≈ 2.5) and FSR (<3.1) under stable combustion conditions were much lower. The combustion behavior of TPO has partial similarity with unsaturated hydrocarbons and ester biofuels. The reported results support the well-characterized TPO condensates for subsequent atomized combustion in realistic industrial burners.

1. Introduction

Tire is a category of widely used rubber consumable. Scrap tires occupy a large amount of land resources, breed mosquitoes to spread diseases, and cause fire disasters, so they are defined as a typical black pollution. In total, 1.5 billion tires are scrapped worldwide every year; in other words, more than 4 million tires are scrapped per day on average [1]. The European Union (EU) issued a ban in 2003 to prohibit the disposal of waste tires in landfills due to the long natural degradation time and the harm of toxic components, including heavy metals (Mn, Cr, Pb, etc.) to soil, plants, and groundwater [2–5]. For these environmental reasons, traditional disposal technologies such as direct incineration and landfills are not appropriate for waste tires [6]. Converting unrecyclable waste tires into alternative oil fuel is a very attractive method to solve the pollution problem caused by millions of tires. In contrast with traditional ways, biodegradation and pyrolysis are universally considered two effective and environmentally friendly disposal methods. The former enhances the nitrification of polymer degradation through nitrifying-enriched activated bacterial communities [7] while the latter has been highlighted in several works [8–11].

The pyrolysis of waste tires at atmospheric pressure is usually performed in an inert atmosphere (N_2, Ar, He, et al.) at moderate temperatures of 400–800 °C. Raw materials are transformed into light noncondensable gas, tar and solid carbon black through thermal decomposition for a period of time [12]. One of the major products is tire pyrolysis oil (TPO), which is usually applied in energy conversion processes as a valuable fuel due to its high calorific value (40–44 MJ) [13]. Like bio-oil, TPO with practicality and economic feasibility has received widespread attention and introduced a wide range of commercial prospects. Diverse studies address the production and application of mixed fuels through the pyrolysis of waste tires.

Yaqoob et al. [14] provided a detailed overview of the potential of TPO as an alternative fuel for diesel engines, which involved applications related to TPO purification and physicochemical properties. In the

* Corresponding author.
E-mail address: hqx@zju.edu.cn (Q. Huang).

https://doi.org/10.1016/j.fuproc.2021.107093
Received 8 September 2021; Received in revised form 2 November 2021; Accepted 7 November 2021
Available online 11 November 2021

process of combining extraction and adsorption, sulfur in TPO can be significantly reduced [15,16]. The methods of blending raw TPO with two additives (natural zeolite and lime) in different mass ratios, hydrodeoxygenation, cracking, and blending TPO with diesel, biodiesel (or other fuel) with or without using additives and nanoparticles [17] as novel fuels have been proven to be effectual in motivating compression ignition diesel engines to work. Various mixtures in the diesel engine were tested, and good capability was obtained for low-sulfur tire fuel oils [18]. These studies explored the performance of TPO from the perspective of environmental improvement and tested the properties of diesel engines while using TPO blended fuels without involving its own combustion behavior.

At present, single-particle combustion is the most common method to study the combustion characteristics of liquid fuels. Based on single droplets, Wang et al. [19] explored the flame diffusion and combustion characteristics of two adjacent drops of jatropha oil under atmospheric pressure and room temperature (300*K*). In addition to biofuels, single-droplet combustion is typically adopted in studies of petroleum oil combustion characteristics and their derivatives [20–23]. Sun et al. [24] conducted a microgravity experiment of polyethylene (PE) pyrolysis oil droplet combustion on a 3.6-s descending tower with a gravity of 10^{-3}–10^{-4} g and calculated the mass loss rate of the fuel and the fiery heat release rate under microgravity. Muelas et al. [13] immersed a sort of free-falling small waste tire oil droplets (150 μm) into the airflow to simulate the actual combustion flame of a one-dimensional structure.

Tires are mainly divided into semi-steel tires and full-steel tires according to the material and structure. The former is primarily made from natural rubber (polyisoprene), whereas the latter is primarily made from synthetic rubber (butylbenzene and butadiene). In order to improve the pyrolysis efficiency of waste tires and flash point of condensed oil products as much as possible, optimize the quality, and combust more specifically, this experiment about analyzing combustion characteristics of new TPOs in different condensing cases was established as a data support for more specific atomization burner designs.

Herein, natural rubber tire pyrolysis oil (NRTO) and synthetic rubber tire pyrolysis oil (SRTO) were selected as typical TPOs. GC/MS was utilized to analyze the chemical components of TPOs. TGA and single-droplet combustion experiments were performed to study the combustion behavior at different condensation temperatures (25 °C and 130 °C) by calculating the thermodynamic energy and capturing droplet combustion images for the quantitative analysis and to provide a reference for the liquid mist combustion of TPO in engineering applications for the first time.

2. Material and method

2.1. Preparation and properties of pyrolysis oil

The raw materials of waste tires used in this research were provided by Hangzhou Zhongce Rubber Industrial, and the results of approximate and ultimate analysis are shown in Table 1.

Table 1
Technical, elements and calorific value analysis of waste tire.

	Properties	Value	
		NRT	SRT
Industrial analysis	Moisture, ad%	1.59	1.42
	Ash, ad%	10.17	10.39
	Volatile, ad%	61.68	61.70
	Fixed carbon, ad%	26.56	26.49
Element analysis	C, ad%	79.88	79.11
	H, ad%	5.35	5.11
	O, ad%	0.57	0.95
	N, ad%	0.39	0.72
	S, ad%	2.05	2.30
Calorific value	Qb, ad (MJ/kg)	36.1	35.9

ad. Air dry base.

The pyrolysis reaction was conducted in a stepped pyrolysis furnace with continuous feeding. Apparatus and internal twin-screw structure diagram are shown in Fig. 1.

Processing capacity of the twin-screw continuous reactor is 10 kg/h under a temperature gradient of 425, 450, 475 °C. The whole system mainly includes feeding device, pyrolysis system, gas discharging lock and pyrolysis oil condensation facility. Resistive radiation heating is adopted to precisely control the temperature of the pyrolysis furnace, and 12 silicon-carbide rods are evenly distributed inside the furnace to ensure uniform heating of the pyrolysis chamber. The pyrolysis furnace is designed as a form of double spiral, which can prevent the scrap tire particles from adhesion due to heat. The transmission speed of the screw is adjustable by frequency conversion to ensure that the pyrolysis time of rubber in high temperature heating section is maintained at 5 min. Exhaust port is connected with a vacuum pump, and pressure in the furnace is controlled at about −30 Pa. In this case, pyrolysis combustible gas will not leak out and can be quickly discharged, reducing the secondary pyrolysis reaction. Finally, the pyrolysis gas is condensed by a temperature-controllable circulating oil cooling system to obtain pyrolysis oil with different flash points.

Four condensed oil samples of NRT and SRT were obtained at 130 °C and 25 °C, respectively. Both temperature and pressure data of the whole process were collected by an Agilent data acquisition instrument. Samples of TPO were centrifuged at a speed of 3000 r/min for 10 min after being sealed and stored for 90 days at 25 °C, preparing for GC–MS analysis. The flash point and density of TPO are shown in Table 2.

The chemical composition of TPO was analyzed by GC/MS-QP2010 SE (Shimadzu, Japan), using SH-Rxi-5sil MS capillary column (30 m × 0.25 mm inside diameter ×0.25 μm film thickness). Initial oven temperature of 40 °C was maintained for 5 min, then heated up to a final temperature of 300 °C at a rate of 10 K/min. After maintaining for 10 min, the chromatographic column began to cool down. The carrier gas was He (analytically pure quality) at a constant column flow of 1.01 mL/min. Temperatures of the injector, source of ion and connector were controlled at 300 °C, 250 °C, 280 °C, respectively. Samples volume of 1 μL (100 μL diluted to a final volume of 3 mL in a mixture of CH_2Cl_2) were injected applying a 10:1 split mode. Each integrated peak detected was automatically searched in the library, previously being defined in NIST 2016. It was supposed that the whole sample was eluted and analyzed in the GC–MS chromatogram. The semi-quantitative test results are shown in Table 3-4.

2.2. Droplets combustion device

A self-designed single-droplet combustion device was used to characterize the evaporation and combustion process of TPO. The entire facility refers to the literature [25], and the specific structure is shown in Fig. 2.

The combustion experiments were performed in a 0.28 m^3 stainless-steel cavity. Optical quartz glass was embedded in the front and back of the cavity for easy measurement. In order to support the droplets and prevent excessive heat exchange with them, a ceramic wire was selected. Compared with the droplet size, the volume of the sealed chamber is large enough so that natural convection influence of air on droplets combustion can be ignored. A micro-injector was used to generate a 1.6 ± 0.02 μL of ellipsoid fuel droplets and hang it to the tip of the ceramic wire. The diameter of the ceramic wire is much shorter than 10% of the droplet size. It can be approximated that the droplet deformed due to its own gravity and the influence of ceramic wire on the droplet during combustion process is able to be neglected [26]. A time-delay electromagnetic relay with a resolution of 0.01 s controlled the ignition time, and the current flowing through the heating wire during ignition was maintained at about 3 A.

A black/white high-speed CCD camera with a Sigma 105 mm macro lens, a frequency of 2000 frames, and an exposure time of 200 μs, was

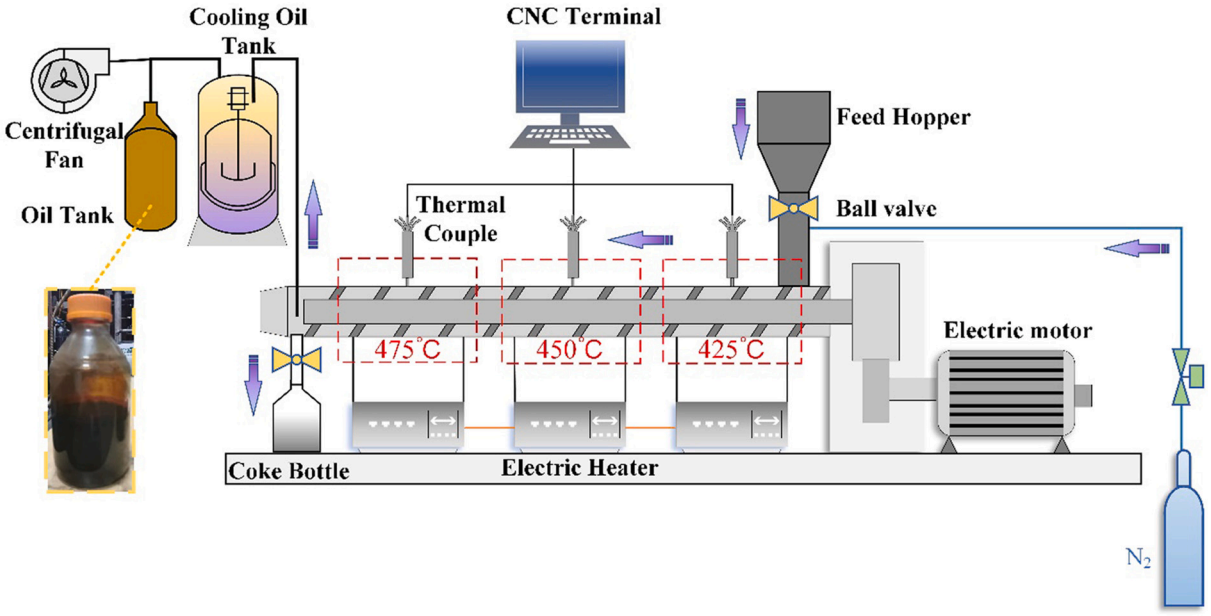

Fig. 1. Equipment structure diagram.

Table 2
Flash point and density of TPO.

	Properties	Value[a]	
		NRTO	SRTO
Flash point (GB/T 261–2008)	25 °C condensation (°C)	<30	<30
	130 °C condensaton (°C)	42.5	52.5
Density (20 °C)	Kg/m^3	917.4	929.5

[a] As received.

Table 3
Properties of NRTO.

	25 °C		130 °C	
	Main substance	Peak area (%)	Main substance	Peak area (%)
C_6H_{6-12}	benzene	1.29	–	–
	Hexene	8.22		
C_7H_8	Toluene	7.32	Toluene	2.1
C_8H_{8-10}	Xylene	5.84	Xylene	3.41
	Ethylbenzene	2.35	Octene	4.6
	Octene	5.0		
C_9H_{12}	Trimethylbenzene	2.4	Trimethylbenzene	0.95
	1-methyl, 2-ethyl - benzene	7.84	Olefin	0.96
$C_{10}H_{12-18}$	Limonene	33.81	Limonene	45.05
	Olefin	14.92	Olefin	13.03
	Sulfurous acid ester	0.56	Sulfurous acid ester	5.11
Others	Alkanes (C > 10)	2.13	Alkanes (C > 10)	3.95
	Aminobenzene	1.61	Olefin (C > 10)	3.4
			Aminobenzene	4.47

used to capture the entire burning process of droplets. The photos were processed by ImageJ software to evaluate the droplet diameter, and the maximum uncertainty in droplet diameter measurement was estimated to be less than 10% [27].

Although the actual shape of the droplet is ellipsoidal, its eccentricity is less than 0.2 according to image analysis of Fig. 3, so the following equivalent spherical volume formula can be used to approximate the droplet diameter:

Table 4
Properties of SRTO.

	25 °C		130 °C	
	Main substance	Peak area (%)	Main substance	Peak area (%)
C_6H_{8-10}	Hexadiene	1.34	–	–
	Cyclohexadiene	0.53		
C_7H_8	Toluene	2.06	–	–
C_8H_{10}	Xylene	3.65	Xylene	2.4
	Limonene	47.18	Limonene	43.63
$C_{10}H_{12-18}$	Olefin	22.45	Olefin	15.46
	P-methyl-1 methyl ethyl benzene	5.83	*P*-methyl-1 methyl ethyl benzene	7.58
	Sulfurous acid ester	2.56	Sulfurous acid ester	5.5
Others	Alkanes (C > 10)	4.54	Alkanes (C > 10)	5.06
	Olefin (C > 10)	1.55	Olefin (C > 10)	4.62
	Aminobenzene	2.38	Aminobenzene	6.03

$$V = \frac{1}{6} \times \pi \times d_h \times d_w^2 = \frac{1}{6} \times \pi \times d^3 \quad (2\text{-}1)$$

where d_h is the long diameter of the ellipse in Fig. 3, d_w is the short diameter of the ellipse, d is the diameter of equivalent sphere.

A ceramic rod with a standard outer diameter of 0.2 mm was utilized as a suspension support in order to regard it as a reference for calibrating droplet and flame size by adjusting the DPI (≥600), brightness, gray-scale and saturation of the entire picture until each pixel was evidently distinguished. The relationship between actual size of the image and pixels was approximately 1:36, accordingly the scale of each clear graph can be obtained.

3. Results and discussion

3.1. Combustion kinetic analysis by Coats-Redfern method

Fig. 4 shows that the TG-DTG curves of NRTO and SRTO (20 mg) rise from the initial temperature of 60 °C to 820 °C at a rate of 20 K/min (carrier gas: air, 50 mL/min; protective gas: N_2, 20 mL/min). Long-term experiments have proven that the classical chemical reaction kinetics Arrhenius Eq. (3-1) is applicable to both solid-phase reactions and most

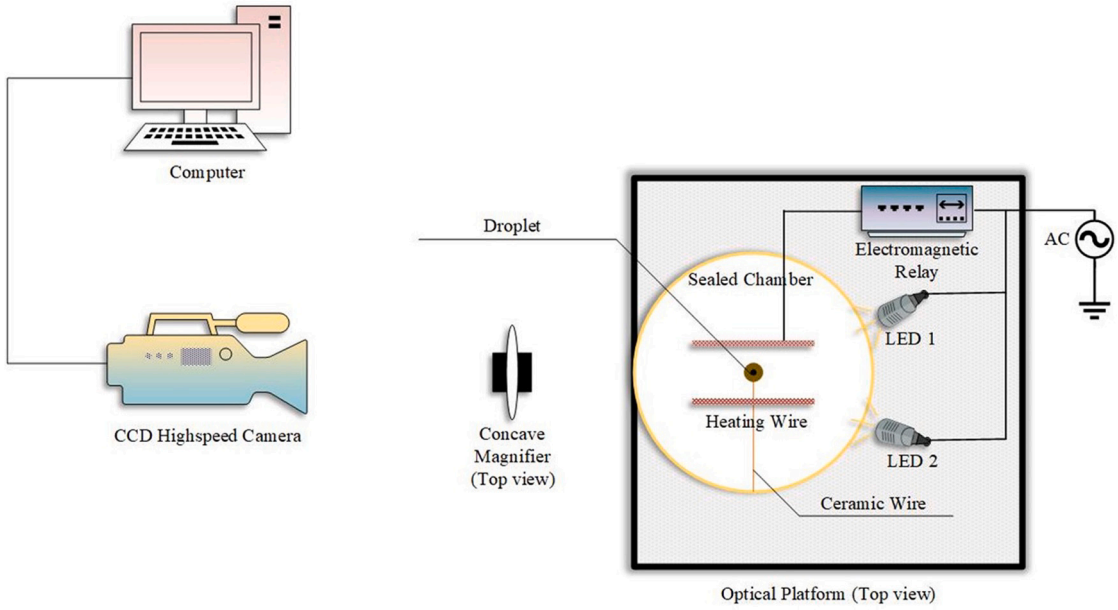

Fig. 2. Schematic of experimental setup.

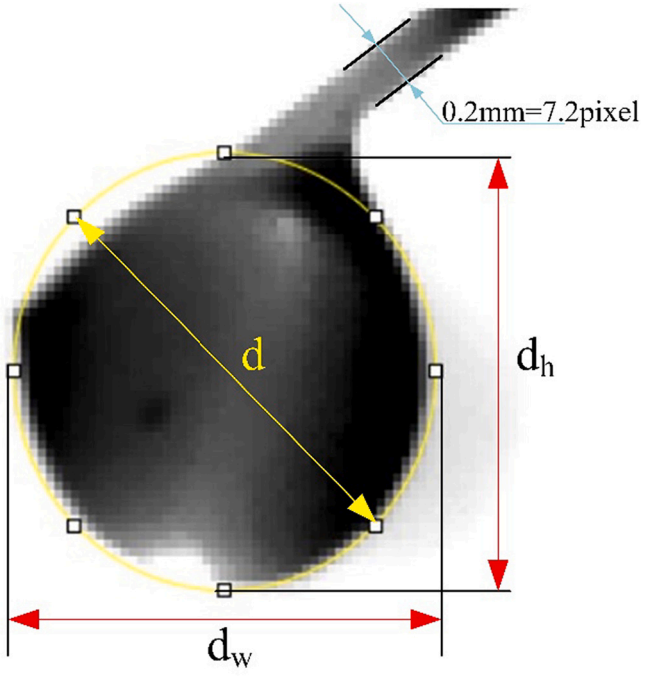

Fig. 3. Size measurement of oil droplet.

liquid- and gas-phase reactions.

$$K(T) = A\exp\left(-\frac{E_\alpha}{RT}\right) \tag{3-1}$$

Based on Arrhenius equation, the total reaction rate of the fuel pyrolysis process is usually characterized by Eq. (3-2).

$$\frac{d\alpha}{dt} = K(T)f(\alpha) \tag{3-2}$$

where α represents the weight loss rate during thermal conversion, t is heating time, K(T) is the function expression of pyrolysis reaction rate with temperature, f(α) means the preset reaction mechanism function, and g(α) is the integral form of f (α) [28].

The International Federation of Thermal Analysis and Calorimetry (ICTAC) recommended multi-step model fitting methods for complex reactions in 2020 [29], among which Coats-Redfern method (C-R) [30] is a general overall model-fitting method that is widely used to determine single-step and multi-step reaction models for carbonaceous materials. Substituting Eqs. (3-1) into (3-2) and transposing, we obtain the parameter estimation of the reaction kinetic expression of C-R method as follows:

$$ln\left[\frac{g(\alpha)}{T^2}\right] = ln\frac{AR}{\beta E_\alpha} - \frac{E_\alpha}{RT} \tag{3-3}$$

A linear regression equation between $\frac{g(\alpha)}{T^2}$ and $\frac{1}{T}$ is established by the function drawing tool Origin, while activation energy E_α and pre-exponential factor A can be obtained through the slope and intercept of the regression line, respectively.

As previously mentioned, the thermal degradation process of TPO under air conditions can be roughly divided into two stages according to the DTG curve. The kinetic parameters in Table 5 and Table 6 are calculated using different reaction models based on thermogravimetric data. The results demonstrate that an evident distinction in the apparent activation energy (Eα) and pre-exponential factors (A) calculated by different reaction model functions (g(α)). Completely different kinetic parameter values are observed when the same reaction mechanism function is applied to different weight loss stages, which confirms the existence of a multi-stage dominant kinetic process [28].

The correlation coefficient (R^2) of the fitting equation at each stage is greater than 0.9, which indicates that the use of the C-R integration method to calculate the kinetic parameters of TPO gains a credible effect. In stage I, the fitting results of the 2nd-order reaction function models ($g(\alpha) = [-\ln(1-\alpha)]^2$ and $g(\alpha) = [(1-\alpha)^{-2}-1]/2$) are highly consistent, while the reactions in stage II are more complicated because many small peaks appear in the DTG curve. Reference [31] states that the apparent activation energy range of the first-stage evaporative combustion weight loss of oil fuels is generally 30-70KJ/mol. Chemical reaction is much easier to proceed at high temperatures, indicating that Eα of stage II oxidation reaction will be lower. In stage I, the oxidation reactions of -CH and -NH radicals mainly occur, whereas the oxidation of -NO is dominant in stage II of SRTO due to its higher nitrogen content. Therefore, the main reaction order of stage II (SRTO) is 3 while others

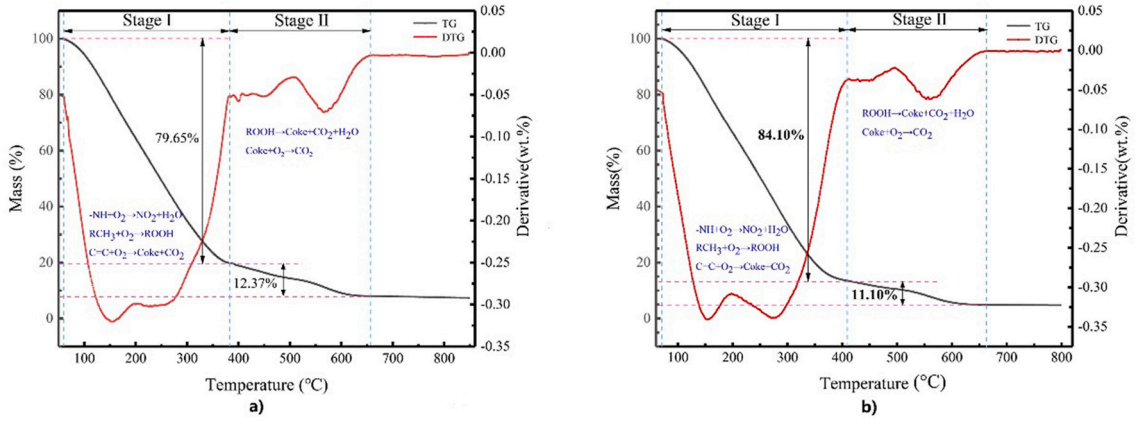

Fig. 4. TG-DTG curves of NRTO (a) and SRTO (b).

Table 5
Calculation results of Eα and A (NRTO) by C-R method.

		Stage I (60–380 °C)			Stage II (380–660 °C)		
Mechanism function g(α)	Reaction order (n)	Eα (KJ/mol)	A (min^{-1})	R^2	Eα (KJ/mol)	A (min^{-1})	R^2
−ln(1-α)	1	11.413	0.927	0.9807	–	–	0.979
$[-\ln(1-\alpha)]^2$	2	31.434	175.1	0.998	–	–	<0.9
$[-\ln(1-\alpha)]^3$	3	51.455	19,650.6	0.9949	8.499	0.966	0.9478
$[(1-\alpha)^{-2}-1]/2$	2	28.951	367.6	0.9868	13.266	10.3	0.9715

R^2. Correlation coefficient of fitted equation.

Table 6
Calculation results of Eα and A (SRTO) by C-R method.

		Stage I (60–410 °C)			Stage II (410–660 °C)		
Mechanism function g(α)	Reaction order (n)	Eα (KJ/mol)	A (min^{-1})	R^2	Eα (KJ/mol)	A (min^{-1})	R^2
−ln(1-α)	1	14.207	2.191	0.9946	–	–	<0.9
$[-\ln(1-\alpha)]^2$	2	37.174	771.2	0.9981	–	–	<0.9
$[-\ln(1-\alpha)]^3$	3	60.142	167,837.6	0.9987	15.772	10.1	0.9379
$[(1-\alpha)^{-2}-1]/2$	2	37.337	3508.5	0.9751	32.519	1320	0.9134

R^2. Correlation coefficient of fitted equation.

are all 2. Referring to the literature [31,32], it is eventually confirmed that Eα for the reaction of NRTO is close to 31.4 KJ/mol (60–380 °C) and 13.3 KJ/mol (380–660 °C); Eα of SRTO is close to 37.2 KJ/mol (60–410 °C) and 15.8 KJ/mol (410–660 °C), which is similar to the air-stream combustion kinetic parameters of acetol bio-oil (14.5–50.1 KJ/mol).

3.2. Droplet and flame shapes

The GC/MS characterization results reflect that TPO is a complex pyrolysis liquid mixed with various carbon-based compounds with large molecular weight differences (C_6-C_{15}). When one compares fuels, a significant difference lies in the appearance of microexplosions of NRTO (25 °C) and SRTO(25 °C), whereas the other fuels, including NRTO (130 °C) and SRTO(130 °C), smoothly evaporated until the droplet

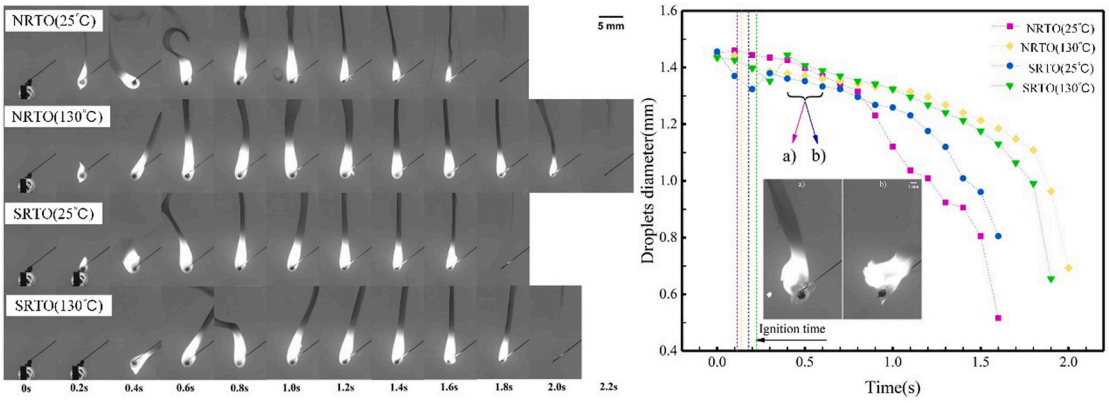

Fig. 5. Combustion process and micro-explosion of TPO captured by high-speed CCD camera: a) NRTO(25 °C); b) SRTO(25 °C).

disappears. Despite the obvious differences in composition of liquid, the phenomenon of microexplosions concur in [21,23] in the combustion of bio-oil. It is worth noting that there exists heterogeneous nucleation on the solid-liquid surface in suspended combustion system, which means stable components crystallize or form a film coating on the surface of a two-phase immiscible medium, typically, production of bubbles on solid walls. In addition to the ceramic wire in this experiment, since it can be used as a heterogeneous nucleation site [13], the huge difference in volatility of each compound in TPO condensed at room temperature may also cause its microexplosive characteristics. Figs. 5 a) and b) show the obvious microexplosion in the initial stage (0.4–0.6 s) of NRTO (25 °C) and SRTO (25 °C).

Microexplosion is accompanied by severe wrinkles and deformation on the surface of the droplet, which is consistent with the PE droplet combustion model in [24]. Unlike traditional fuels, pyrolysis oil fuels are often mixed with micron-level or larger carbon black particles, which are produced during high-temperature pyrolysis. According to previous literatures [13,26], heterogeneous nucleation occurs between the solid phase and the liquid phase. To better verify the effect of solid carbon black on the burst of pyrolysis oil, the SRTO (25 °C) with more obvious microexplosion phenomenon was selected as the object. Organic filter paper (0.22 μm) was utilized to percolate the original oil sample, and combustion conditions of 3 mL fuel before and after filtration were observed by a digital camera.

The results are shown in Figs. 6 A) and B). Filamentous sparks burst in a short time after the unfiltered liquid was ignited, whereas the filtered fuel stably combusted in the porcelain boat. The uneven flame front reflects that the solution was not completely homogeneous; nevertheless, the liquid did not spray out again after being filtered, which indicates that the difference in boiling point and solute distribution of the multiple components present does not significantly promote the bursting of TPO. The most likely situation is that during the heating process, heterogeneous gasification cores formed between the contact surface of the carbon black and the liquid phase inside the droplet, which accelerates the bubble generation. Bubbles moved to the surface of the droplet, cracked due to the pressure difference, and caused microexplosions, as shown in Fig. 6.

3.3. Burning rate and flame stand-off ratio

The characteristics of the combustion process were analyzed in more detail based on Fig. 5 to extract the varieties of droplet and flame size over time, scilicet the burning rate, ignition delay, total combustion time and flame stand-off ratio (FSR). Real burning conditions of droplets in the air were simulated without additional oxygen injection into the chamber. Tests of the same fuel oil were performed more than three times to check the repeatability of each experimental procedure. Since the response delay time of the electromagnetic relay is less than 0.01 s, its impact on the ignition time is considered to be within the acceptable error range of the experiment. From the statistical results, the relative differences calculated in burn-out time and ignition time of the same droplets did not exceed 4.9% and 3.4%, respectively.

The droplet diameter evolution curves captured by the CCD camera at an interval of 0.1 s were processed and are presented in Fig. 7. The evaporation section (the first 0.2 s) involved the thermal expansion of droplets and evaporation of low-boiling substances separated from the oxidized surface. The former positively promoted the extension of droplet diameter, while the latter negatively inhibited the development of droplet size. Only NRTO(25 °C) significantly inflated before ignition, which illustrates that the movement of bubbles inside its liquid film is dominant compared to the evaporation behavior of components with low boiling points. The volume of SRTO abruptly increased after being ignited, which could be attributed to the expansion of molecular gaps caused by the free radical detachment of high-carbon cyclic and breaking of chain hydrocarbons after the combustion exotherm. After ignited, the rate of SRTO droplets surface evaporation is much lower than that of boundary expansion caused by internal groups thermal movement. The volume of STRO reached the maximum value when the combustion system was in dynamic equilibrium, and then droplets shrank due to the increase of temperature and evaporation rate.

The literature [33] found that for the steady combustion of idealized uniform droplets, the square of diameter linearly changes with time in a completely stable burning state. After an apparent heating-up transient period, the variation in d^2 with time gradually tended to a constant slope, which is called the burning rate (represented by K). For more in-depth insight into the relevant parameter of d^2, d^2-t curves of relatively stable combustion were fitted to a 5th-order polynomial function, whose derivative described the function of burning rate and time: $K = -\frac{d(d^2)}{dt}$. The results are shown in the right column of Fig. 7. Contrary to the notion of the d^2-law, the time-independent parameter K of all d^2-t curves continued to increase to a quasi-stable value.

This phenomenon is predictable, since the liquid phase exhibits homogenization during the lifespan of droplets, which is ascribed to the

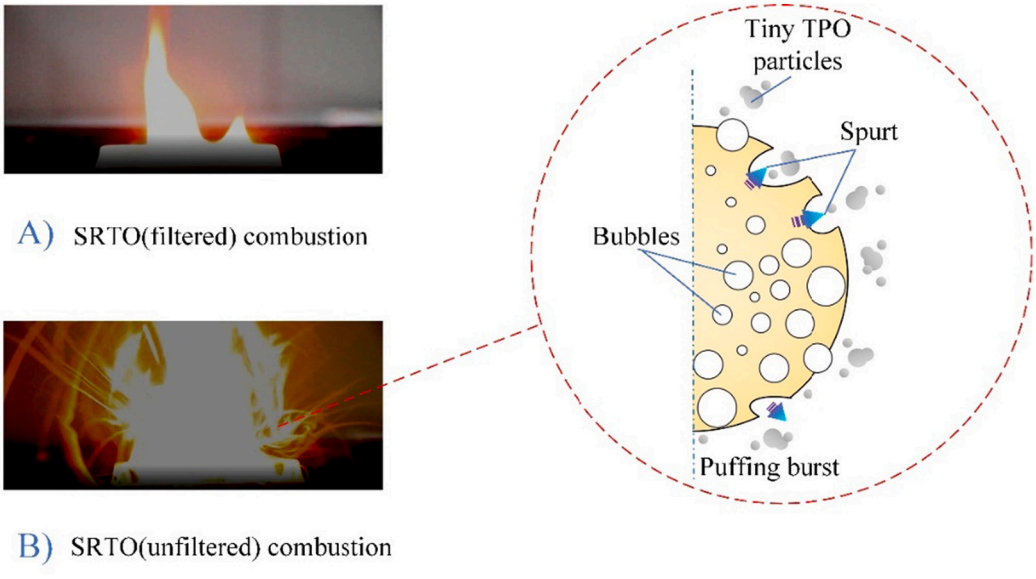

Fig. 6. Schematic diagram of TPO droplets nucleation and bursting process.

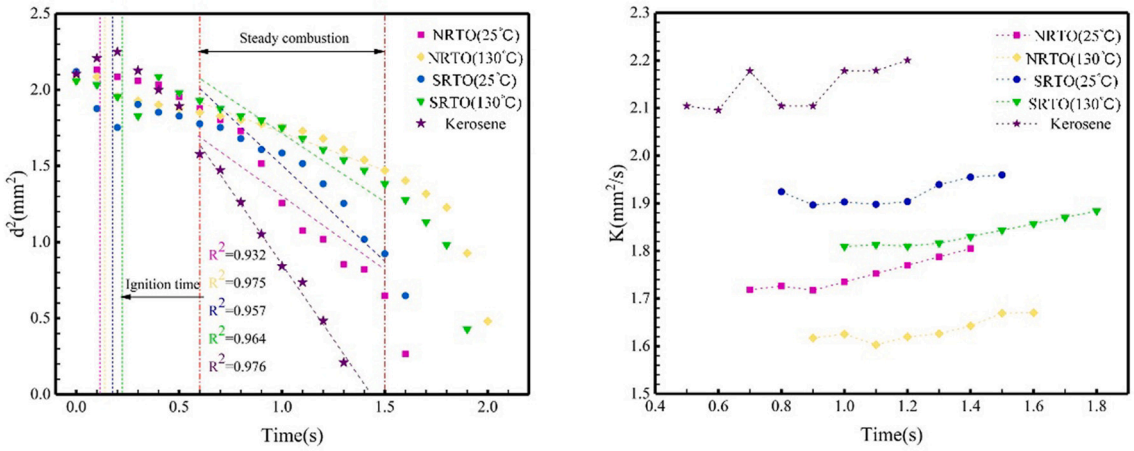

Fig. 7. Evolution and differential curves of droplet size for NRTO(25 °C), NRTO(130 °C), SRTO(25 °C), SRTO(130 °C) and Kerosene.

constant decomposition of macromolecules into smaller particles. The decomposition process is generally accompanied by the swelling phenomenon in initial stage of heating. Production of smaller molecules and intensification of irregular thermal movement led to inflation, surface wrinkles and a sharp increase in the effective contact area between droplets and the air, which significantly promoted diffusion combustion.

From the data of the differential curve, the burning rates of 4 pyrolysis oils in the steady combustion stage (0.6 s–1.5 s) approach 1.76 ± 0.03 mm^2/s, 1.63 ± 0.03 mm^2/s, 1.93 ± 0.03 mm^2/s, 1.84 ± 0.03 mm^2/s for NRTO(25 °C), NRTO(130 °C), SRTO(25 °C) and SRTO(130 °C), respectively, which are lower than K of standard kerosene under atmospheric pressure (2.15 ± 0.05 mm^2/s according to [25]), precisely due to the higher C/H ratio of TPO. In sharp contrast with standard kerosene, n-hexadecane, butanol and other traditional fuels, the saturated hydrocarbon content of TPO is less than 10%. In fact, aromatics and olefins in kerosene are less than 6%, while the unsaturation degree of butanol is 0. Therefore, the relatively higher saturation of hydrogen atoms provides a proper interpretation for the shorter burnout time of SRTO compared with NRTO. In addition, the higher burning rate (K) at 25 °C than that at 130 °C can be explained by the micro-explosion, which has been elaborated before, and smashes a considerable fraction of the droplets in advance. Otherwise, the relatively stable combustion behavior suppresses the burnout of droplets, especially for NRTO (130 °C).

The burning-rate constant (K) depends on the processes of phase change and mass transfer. The classical expression of the mass-transfer number (B) can be applied for the TPO droplet as:

$$B_{TPO} = \frac{\frac{\Delta h_c}{\nu} + c_{pg}(T_f - T_{py})}{\Delta h_{py}} \approx 2.5 \tag{3-4}$$

where $\Delta h_c \approx 42$ MJ/kg is the heat of combustion; $\nu = 13.46$ is the stoichiometric air-fuel ratio [13]; $\Delta h_{py} \approx 1.95$ MJ/kg is the pyrolysis heat of the solid scrap tire; $c_{pg} \approx 2$ KJ/kg-K is the specific heat of fuel. $T_f \approx 1473$ K and $T_{py} = 698$ K are the average temperature of the combustion flame and pyrolysis, respectively.

The value of B_{TPO} is much smaller than that of heptane (B ≈ 8.5) and diesel (B ≈ 11) [14], since the pyrolysis temperature of waste tires (T_{py}) in formula (3-5) is much higher than the gasification temperature of most traditional liquid polymer fuels, which results in a steep increase in heat desorption (Δh_{py}). In addition, for liquid polymer fuels, the surface temperature continues to increase even above the pyrolysis point with strong internal heat convection. The fuel mass loss rate (m'_f) and mass flux (m''_f) increase with B [24] as:

$$m'_f = \frac{\pi}{4}\rho_l K d = \frac{2\pi k_{l-g} d}{C_{pg}} ln(1+B) \tag{3-5}$$

$$m''_f = \frac{\rho_l K}{4d} = \frac{2k_{l-g}}{dC_{pg}} ln(1+B) \tag{3-6}$$

where ρ_l is the density of the liquid fuel; k_{l-g} is the local thermal conductivity of the gas-liquid interface during combustion; K is the combustion rate constant; B is the mass transfer number. The obtained K values of the 4 TPO droplets are substituted into Eqs. (3-5) and (3-6), and the results are displayed in Table 7. Compared to common bio-oils, methyl myristate, methyl laurate methyl caprate measured in [33,34] and PE (liquid) in [24], TPO at room temperature (293 K) has a much higher calculated k_{l-g}, which indicates that greater heat transfer and evaporation efficiency can be obtained when TPO is selected as a fuel.

The flame stand-off ratio (FSR = $\frac{d_f}{d}$) is widely acknowledged as a crucial indicator to evaluate flame diffusion behaviors in droplet combustion. Sooty flames captured by a high-speed CCD camera were post-processed by ImageJ to quantify the comet flame radial development with time. The practical FSRs are displayed in Fig. 8 and show similar behaviors of the 4 TPOs (NRTO (25 °C), NRTO (130 °C), SRTO (25 °C), SRTO (130 °C)). After being ignited, the flame size of all four pyrolysis oils sharply fluctuated due to deflagration, whereas the NRTO (130 °C) exhibited a short-term lag of approximately 0.2 s. This experimental result is attributed to the accumulation of fuel vapor near the droplet, and the deflagration effect will be considerably weakened when the oxygen concentration in the blended gas co-flow is low. OH and O radicals become enriched with the increase of intake oxygen concentration [35]. In a certain interval, as the oxygen concentration decreases, the effective contact area of fuels and oxygen radicals shrink, resulting in simultaneous carbonization and oxidation of fuel, and higher soot volume fraction. Under this condition, the fuel will not be completely ignited at once even if the temperature reaches the ignition point, and the deflagration effect is suppressed. As described in the literature [13], the first appearance of a measurable flame is delayed when the oxygen availability decreases.

Table 7
Mass loss rate, mass flux and local thermal conductivity of fuels.

Droplets	m'_f(kg/s)	m''_f(kg/(m²•s))	k_{l-g}(w/(m•K))[a]
NRTO(25 °C)	1.93×10^{-9}	2.92	0.326
NRTO(130 °C)	1.78×10^{-9}	2.62	0.302
SRTO(25 °C)	2.11×10^{-9}	3.11	0.358
SRTO(130 °C)	2.01×10^{-9}	2.96	0.341
PE(Liquid)		4 ± 1	0.23
Methyl myristate			0.146–0.155
Methyl laurate			0.142–0.151
Methyl caprate			0.138–0.142

[a] 20 °C.

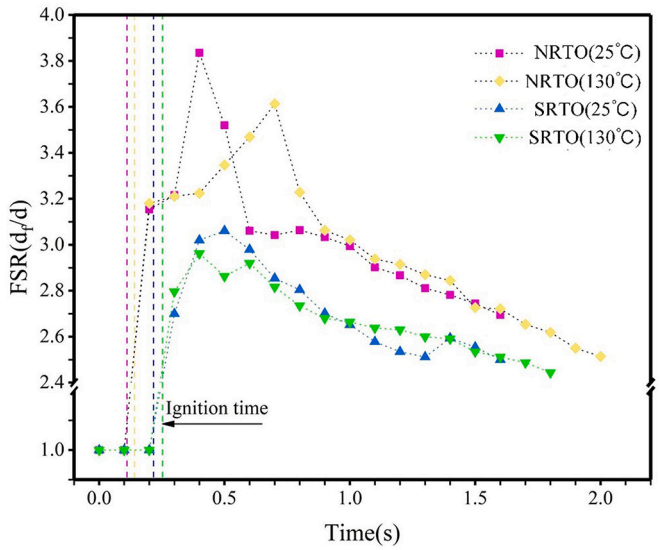

Fig. 8. Flame stand-off ratio evolution for TPO.

Referring to the theory described above, the lower FSR value of SRTO can be attributed to its higher carbon content (C ≥ 10 on average), which generates fewer oxygen-contact sites when the amount of oxygen is fixed. An unexpected increase occurs in the SRTO(25 °C) FSR curve (1.4 s), since the decomposition and carbonization of high-carbon substances induces the formation of microexplosions. Except for the deflagration phase, the FSR of all 4 TPOs is basically lower than 3.1 compared with polyethylene (4–5, according to [24]) and methanol (5–6, according to [36]), which implies that it is difficult to achieve better TPO combustion conditions without increasing the excess air coefficient.

4. Conclusions

In this paper, a pilot-scale continuous auger reactor was used to conduct pyrolysis and condensation experiments on waste tire particles to produce tire pyrolysis oil (TPO). Subsequently, the combustion kinetic parameters of natural rubber tire pyrolysis oil (NRTO) and synthetic rubber tire pyrolysis oil (SRTO) were calculated using the TGA curves and C-R method. Meanwhile, the combustion characteristics of 1.6-μL oil droplets condensed at 25 °C and 130 °C were extracted using a droplet combustion device and compared with other fuels. The results are as follows:

1) The apparent activation energy (Eα) for the reaction of NRTO and SRTO is close to 31.4 KJ/mol (60–380 °C), 13.3 KJ/mol (380–660 °C) and 37.2 KJ/mol (60–410 °C), 15.8 KJ/mol (410–660 °C), respectively, which is similar to the alkyne bio-oil combustion;
2) Due to the larger difference in volatility of each compound in TPO condensed at room temperature and the micron-sized carbon particles in the droplet, NRTO (25 °C) and SRTO (25 °C) are more prone to microexplode, which promotes the combustion of oil droplets. In addition, the saturation of SRTO is relatively higher than that of NRTO, which causes higher burning rates (1.93 ± 0.03 mm^2/s) of SRTO (25 °C);
3) TPO has a lower mass transfer number (B ≈ 2.5) than several traditional fuel oils such as heptane and diesel. B is utilized to further obtain the local thermal conductivity (k_{l-g}) of the gas-liquid interface. Surprisingly, value of k_{l-g} (>0.3) presages considerable gasification efficiency for the TPO combustion;
4) NRTO has a higher flame stand-off ratio (FSR) due to its lower carbon content (<10 on average). Nevertheless, TPO droplets have much smaller FSR (<4) than alkane or alcohol fuels, which can be ascribed to the lack of oxygen.

Regarding the two main types of waste tires, the novel pyrolysis and condensation methods illustrated above are considered to effectively improve the pyrolysis efficiency and the quality of oil products. On the one hand, calculation of various TPOs combustion parameters that are rarely studied could provide strong data support for the establishment of combustion models under natural convection conditions. On the other hand, comparison with traditional fuels is of great benefit to the design of specific fuel burners and the optimization on the basis of existing equipment in practical industries.

Original statement

All experiments, graphics, and tables in this article are original. The text is written by the first author, modified by the corresponding author and there is no conflict of interest among all authors.

Author statement

No conflict of interest exists among authors and the division of labor is as follows:

Yiliu Zhong: Pyrolysis and combustion experiment; Writing, original draft preparation and revising.

Jun Xu: Responsible for the production of pyrolysis device; Financial support.

Yuhan Pan: Pyrolysis experiment; Data analysis.

Zhitong Yin: Pyrolysis experiment; Data collation.

Xinwen Wang: Financial support.

Yonggang Zhou: Design of pyrolysis device; Technical support.

Qunxing Huang: Project chief; Editing, modifying and revising.

Declaration of Competing Interest

The authors declare that they have no known competing financial interests or personal relationships that could have appeared to influence the work reported in this paper.

Acknowledgements

The authors would like to greatly acknowledge Key Research and Development Program of Zhejiang Province (2020C03084), National Key Research and Development Program (2018YFC1901300), National Natural Science Foundation of China (Grant No. 51621005) and Shandong Province (2019JZZY020806).

References

[1] M. Sienkiewicz, H. Janik, K. Borzędowska-Labuda, J. Kucińska-Lipka, Environmentally friendly polymer-rubber composites obtained from waste tyres: a review, J. Clean. Prod. 147 (2017) 560–571, https://doi.org/10.1016/j.jclepro.2017.01.121.
[2] N. Antoniou, G. Stavropoulos, A. Zabaniotou, Activation of end of life tyres pyrolytic char for enhancing viability of pyrolysis - critical review, analysis and recommendations for a hybrid dual system, Renew. Sust. Energ. Rev. 39 (2014) 1053–1073, https://doi.org/10.1016/j.rser.2014.07.143.
[3] P. Song, X. Wu, S. Wang, Effect of styrene butadiene rubber on the light pyrolysis of the natural rubber, Polym. Degrad. Stab. 147 (August 2017) (2018) 168–176, https://doi.org/10.1016/j.polymdegradstab, 2017.12.006.
[4] D. Landi, S. Gigli, M. Germani, M. Marconi, Investigating the feasibility of a reuse scenario for textile fibres recovered from end-of-life tyres, Waste Manag. 75 (2018) 187–204, https://doi.org/10.1016/j.wasman.2018.02.018.
[5] M. Labaki, M. Jeguirim, Thermochemical conversion of waste tyres—a review, Environ. Sci. Pollut. Res. 24 (11) (2017) 9962–9992, https://doi.org/10.1007/s11356-016-7780-0.
[6] B. Chen, et al., Disposal methods for used passenger car tires: One of the fastest growing solid wastes in China, Green Energy Environ. xxxx (2021), https://doi.org/10.1016/j.gee.2021.02.003.

[7] A. Sepehri, M.H. Sarrafzadeh, Effect of nitrifiers community on fouling mitigation and nitrification efficiency in a membrane bioreactor, Chem. Eng. Process. Process Intensif. 128 (March) (2018) 10–18, https://doi.org/10.1016/j.cep.2018.04.006.
[8] M. Arabiourrutia, G. Lopez, M. Artetxe, J. Alvarez, J. Bilbao, M. Olazar, Waste tyre valorization by catalytic pyrolysis – a review, Renew. Sust. Energ. Rev. 129 (July 2019) (2020) 109932, https://doi.org/10.1016/j.rser.2020.109932.
[9] T. Menares, J. Herrera, R. Romero, P. Osorio, L.E. Arteaga-Pérez, Waste tires pyrolysis kinetics and reaction mechanisms explained by TGA and Py-GC/MS under kinetically-controlled regime, Waste Manag. 102 (2020) 21–29, https://doi.org/10.1016/j.wasman.2019.10.027.
[10] J. Xu, et al., High-value utilization of waste tires: a review with focus on modified carbon black from pyrolysis, Sci. Total Environ. 742 (2020) 140235, https://doi.org/10.1016/j.scitotenv.2020.140235.
[11] E. Yazdani, S.H. Hashemabadi, A. Taghizadeh, Study of waste tire pyrolysis in a rotary kiln reactor in a wide range of pyrolysis temperature, Waste Manag. 85 (2019) 195–201, https://doi.org/10.1016/j.wasman.2018.12.020.
[12] I.I. Enagi, K.A. Al-attab, Z.A. Zainal, Liquid biofuels utilization for gas turbines: a review, Renew. Sust. Energ. Rev. 90 (March) (2018) 43–55, https://doi.org/10.1016/j.rser.2018.03.006.
[13] Á. Muelas, M.S. Callén, R. Murillo, J. Ballester, Production and droplet combustion characteristics of waste tire pyrolysis oil, Fuel Process. Technol. 196 (July) (2019) 106149, https://doi.org/10.1016/j.fuproc.2019.106149.
[14] H. Yaqoob, Y.H. Teoh, M.A. Jamil, M. Gulzar, Potential of tire pyrolysis oil as an alternate fuel for diesel engines: a review, J. Energy Inst. 96 (2021) 205–221, https://doi.org/10.1016/j.joei.2021.03.002.
[15] M. Mikulski, M. Ambrosewicz-Walacik, J. Hunicz, S. Nitkiewicz, Combustion engine applications of waste Tyre pyrolytic oil, Prog. Energy Combust. Sci. 85 (2021) 100915, https://doi.org/10.1016/j.pecs.2021.100915.
[16] R. Serefentse, W. Ruwona, G. Danha, E. Muzenda, A review of the desulphurization methods used for pyrolysis oil, Procedia Manuf. 35 (2019) 762–768, https://doi.org/10.1016/j.promfg.2019.07.013.
[17] A.K. Hossain, P.A. Davies, Pyrolysis liquids and gases as alternative fuels in internal combustion engines - a review, Renew. Sust. Energ. Rev. 21 (2013) 165–189, https://doi.org/10.1016/j.rser.2012.12.031.
[18] W.C. Wang, C.J. Bai, C.T. Lin, S. Prakash, Alternative fuel produced from thermal pyrolysis of waste tires and its use in a di diesel engine, Appl. Therm. Eng. 93 (2016) 330–338, https://doi.org/10.1016/j.applthermaleng.2015.09.056.
[19] J. Wang, et al., Flame spread and combustion characteristics of two adjacent jatropha oil droplets, Fuel 285 (May 2020) (2021) 119077, https://doi.org/10.1016/j.fuel.2020.119077.
[20] G. Singh, M. Esmaeilpour, A. Ratner, Effect of carbon-based nanoparticles on the ignition, combustion and flame characteristics of crude oil droplets, Energy 197 (2020) 117227, https://doi.org/10.1016/j.energy.2020.117227.
[21] P.M. Guerieri, R.J. Jacob, H. Wang, D.J. Kline, M.R. Zachariah, Droplet combustion of kerosene augmented by stabilized nanoaluminum/oxidizer composite mesoparticles, Combust. Flame 211 (2020) 1–7, https://doi.org/10.1016/j.combustflame.2019.07.031.
[22] Y.H. Kuan, F.H. Wu, G.B. Chen, H.T. Lin, T.H. Lin, Study of the combustion characteristics of sewage sludge pyrolysis oil, heavy fuel oil, and their blends, Energy 201 (2020) 117559, https://doi.org/10.1016/j.energy.2020.117559.
[23] M. Ghamari, A. Ratner, Combustion characteristics of diesel and Jet-A droplets blended with polymeric additive, Fuel 178 (2016) 63–70, https://doi.org/10.1016/j.fuel.2016.03.052.
[24] P. Sun, C. Wu, F. Zhu, S. Wang, X. Huang, Microgravity combustion of polyethylene droplet in drop tower, Combust. Flame 222 (2020) 18–26, https://doi.org/10.1016/j.combustflame.2020.08.032.
[25] H. Zhang, et al., Ignition, puffing and sooting characteristics of kerosene droplet combustion under sub-atmospheric pressure, Fuel 285 (August 2020) (2021) 119182, https://doi.org/10.1016/j.fuel.2020.119182.
[26] E. Mura, R. Calabria, V. Califano, P. Massoli, J. Bellettre, Emulsion droplet micro-explosion: Analysis of two experimental approaches, Exp. Thermal Fluid Sci. 56 (2014) 69–74, https://doi.org/10.1016/j.expthermflusci.2013.11.020.
[27] D.L. Dietrich, P.M. Struk, M. Ikegami, G. Xu, Single droplet combustion of decane in microgravity: experiments and numerical modelling, Combust. Theory Model. 9 (4) (2005) 569–585, https://doi.org/10.1080/13647830500256039.
[28] J. Zhang, Y. Ding, W. Du, K. Lu, L. Sun, Study on pyrolysis kinetics and reaction mechanism of Beizao oil shale, Fuel 296 (March) (2021) 120696, https://doi.org/10.1016/j.fuel.2021.120696.
[29] S. Vyazovkin, et al., ICTAC kinetics committee recommendations for analysis of multi-step kinetics, Thermochim. Acta 689 (March) (2020) 178597, https://doi.org/10.1016/j.tca.2020.178597.
[30] J. Coats, A.W. Redfern, Kinetic parameters from thermogravimetric data, Nature 201 (1964) 68–69.
[31] R. Font, M.D. Rey, M.A. Garrido, Kinetics of the combustion of olive oil. A semi-global model, J. Anal. Appl. Pyrolysis 108 (2014) 68–77, https://doi.org/10.1016/j.jaap.2014.05.015.
[32] T.Y. Ahmed, A. Tanksale, A.F.A. Hoadley, A kinetic model for air-steam reforming of bio-oil over Rh–Ni/γ-Al2O3 catalyst: Acetol as a model compound, Int. J. Hydrog. Energy 45 (46) (2020) 24300–24311, https://doi.org/10.1016/j.ijhydene.2020.06.219.
[33] J. Fan, L. Fan, S. Liu, F. Song, Experimental research on the liquid thermal conductivity of mixtures of methyl caprate and ethyl caprate with n-undecane and n-tridecane, J. Mol. Liq. 333 (2021) 115968, https://doi.org/10.1016/j.molliq.2021.115968.
[34] J. Fan, S. Liu, Q. Meng, F. Song, Liquid thermal conductivity of three biodiesel compounds: Methyl myristate, methyl laurate and methyl caprate, J. Chem. Thermodyn. 155 (2021) 106374, https://doi.org/10.1016/j.jct.2020.106374.
[35] Y. Hua, L. Qiu, F. Liu, Y. Qian, S. Meng, Numerical investigation into the effects of oxygen concentration on flame characteristics and soot formation in diffusion and partially premixed flames, Fuel 268 (November 2019) (2020) 117398, https://doi.org/10.1016/j.fuel.2020.117398.
[36] V. Nayagam, Quasi-steady flame standoff ratios during methanol droplet combustion in microgravity, Combust. Flame 157 (1) (2010) 204–205, https://doi.org/10.1016/j.combustflame.2009.09.012.